Meteoritics & Planetary Science 41, Nr 2, 217–232 (2006)
Abstract available online at http://meteoritics.org

Identification of minerals and meteoritic materials via Raman techniques after capture in hypervelocity impacts on aerogel

M. J. BURCHELL[1*], J. MANN[1], J. A. CREIGHTON[1], A. T. KEARSLEY[2], G. GRAHAM[3], and I. A. FRANCHI[3]

[1]Centre for Astrophysics and Planetary Sciences, School of Physical Sciences,
University of Kent, Canterbury, Kent CT2 7NH, UK
[2]Department of Mineralogy, The Natural History Museum, Cromwell Road, London SW7 5BD, UK
[3]Planetary and Space Science Research Institute, The Open University, Milton Keynes MK7 6AA, UK
*Corresponding author. E-mail: M.J.Burchell@kent.ac.uk

(Received 16 September 2004; revision accepted 07 December 2005)

Abstract–Mineral particles analogous to components of cosmic dust were tested to determine if their Raman signatures can be recognized after hypervelocity capture in aerogel. The mineral particles were accelerated onto the silica aerogel by light-gas-gun shots. It was found that all the individual minerals captured in aerogel could be identified using Raman (or fluorescence) spectra. The laser beam spot size was ~5 micrometers, and in some cases the captured particles were of a similar small size. In some samples fired into aerogel, a broadening and a shift in the wave numbers of some of the Raman bands was observed, a result of the trapped particles being at elevated temperatures due to laser heating. Temperatures of samples were also estimated from the relative intensities of Stokes and anti-Stokes Raman bands, or, in the case of corundum particles, from the wave number of fluorescence bands excited by the laser. The temperature varied greatly, dependent upon laser power and the nature of the particle. Most of the mineral particles examined had temperatures below 200 °C at a laser power of about 3 mW at the sample. This temperature is sufficiently low enough not to damage most materials expected to be found captured in aerogel in space. In the worst case, some particles were shown to have temperatures of 500–700 °C. In addition, selected meteorite samples were examined to obtain Raman signatures of their constituent minerals and were then shot into aerogel. It was possible to find Raman signatures after capture in aerogel and obtain a Raman map of a whole grain in situ in the aerogel. It is concluded that Raman analysis is indeed well suited for an in situ analysis of micrometer-sized materials captured in aerogel.

INTRODUCTION

Raman spectroscopy is a well-established method for identifying a wide range of substances, and is an effective technique for characterizing small particles or inhomogeneous solids. In essence, Raman spectroscopy involves measurement of the spectrum of the scattered light when a substance is illuminated by a monochromatic light source, typically a laser. Although most of the scattered light is of unchanged frequency, inelastic scattering produces side-bands on the laser line, due to the exchange of energy with vibrations of the chemical bonds of the sample. The frequency shifts from the laser line are the bond vibration frequencies, and thus the Raman spectrum is a vibrational spectrum, giving a highly characteristic fingerprint of the sample. Identification may be made by matching the spectrum with known reference materials or a database of standard spectra, or the individual bands in the Raman spectrum may be used to infer the presence of particular bonds in a mineral sample by reference to tables of characteristic bond vibration frequencies. For some solids isomorphous substitution of one element by another, as in a mineral series, results in band shifts, and complementary techniques may then also be required for full chemical identification.

As an analytical technique, Raman spectroscopy has the attractive feature that it may be applied without substantial prior sample preparation, and it is usually nondestructive. It is therefore useful for the examination of small, rare, and valuable samples. For some samples (as in the impure alumina samples discussed below), illumination by the laser may also excite fluorescence, and the fluorescence bands may lie in the same spectral region as the much weaker Raman spectrum. In contrast to the light scattering inherent in Raman spectroscopy, fluorescence involves the absorption of photons

due to electronic transitions in the sample, and the subsequent re-emission of frequency-shifted photons. Fluorescence spectra are thus electronic emission spectra, and fluorescence is restricted to samples which absorb at the laser wavelength. In our paper, the difference between fluorescence (emission spectra with an absolute frequency scale) and Raman scattering (spectral peaks shifted from the frequency of the illumination source) is reflected by a different notation: Raman spectra are given in terms of wave number shifts relative to the illuminating laser, whereas all the fluorescence spectra are absolute wave numbers.

Since the 1960s, Raman spectroscopy has increasingly been used as a characterization method by mineralogists, and there are also several applications of Raman techniques to planetary science. For example, Wopenka (1988) used Raman spectroscopy to study interplanetary dust particles collected in the atmosphere. Meteorite samples have also been studied (e.g., Michel-Levy and Lautie 1981; Wopenka and Sandford 1984; Heymann 1987), looking at mineral phases or the presence of carbon. Wang et al. (1999) not only studied Martian meteorites using Raman but also suggested that a microRaman system be deployed remotely on Mars for in situ analysis of minerals. This idea has been developed further by Wynn-Williams and Edwards (2000), who reported that Raman spectroscopy at infrared wavelengths can be used to identify biomolecules (via their pigment and photoprotective mineral contents) in the Antarctic and who also suggested using such a system on Mars to find regolith habitats on that planet. More recently, Popp et al. (2002) studied meteorite samples with a diverse range of surface quality. They found that perhaps 85% of Raman spectra obtained could be assigned to particular minerals, and that in the worst case (most complex surface topography), 60% of spectra could still be assigned to known minerals. The advantage of an analytical tool that requires minimal sample handling and preparation (and hence negligible modification or contamination) is obvious, and it holds particular promise for initial noninvasive examination of valuable extraterrestrial samples such as those returned by sample return missions to asteroids (e.g., 25143 Itokawa to be visited by MUSES-C/Hayabusa, see Kawaguchi et al. (2003) and Fujiwara et al. (1999 and 2004) and comets (e.g., the Stardust encounter with P-Wild-2, see Brownlee et al. 1996, 2003, 2004).

Recently, a new method of collecting samples of extraterrestrial materials has been deployed in space, namely the use of silica aerogel (SiO_2) to capture small dust particles which impact at high speeds, typically many km s^{-1}. Tsou et al. (1988) showed that despite high impact speeds that normally cause vaporization of the particles when they hit a solid, for impacts at several km s^{-1} into aerogel, the particles are captured relatively intact. Previous results on the location of impacted mineral grains by analytical electron microscopy and laser confocal imagery (e.g., Graham et al. 2004) have shown that particles may fragment during penetration, leaving smaller debris scattered along the characteristic impact track. This is in stark contrast to impacts on normal "solids" such as metal or glass, in which little solid material survives, and residues are restricted to melt and vapor condensates (Graham et al. 2001a). The key is that aerogel is a highly porous, low-density material, essentially a dried silica gel (Kistler 1931, 1932). The result of the low density (which can be made less than 10 kg m^{-3}) is that the impactor tunnels into the aerogel target and is slowed relatively gently. The captured particle is thus often found at the end of a relatively long, carrot-shaped track. Since aerogel is transparent, the track and captured particle are easily seen. Several experiments have deployed aerogel capture cells in space and impacts of small (typically less than 100 or even 10 micron) particles have been reported (e.g. Brownlee et al. 1994; Burchell et al. 1999a; Hörz et al. 2000). In addition, the NASA Stardust spacecraft (Brownlee et al. 2003) was launched in 1999 to visit comet Wild-2 in early 2004 and is believed to have captured freshly-emitted dust grains in aerogel at a relative encounter velocity of 6.1 km s^{-1} (Tsou et al. 2003; Tuzzolino et al. 2004). These were returned to Earth in January 2006.

Appropriate analysis techniques need to be applied to the samples captured in aerogel after their return to Earth. For example, Flynn et al. (1996) showed that synchrotron radiation could provide important elemental information from captured grains. Subsequently, Burchell et al. (2001) showed that Raman techniques could be successfully applied to olivine and enstatite particles fired into aerogel in the laboratory at 5 km s^{-1}. Corundum (ruby) and spinel particles also gave strong fluorescence signals that were also characteristic of these minerals after capture in aerogel. This Raman analysis is in situ within aerogel of millimeters thickness, so obviating the need for time-consuming and risky extraction of the captured particles from the aerogel. Later, Graham et al. (2001b) showed that olivine and carbonaceous components within grains of the CV3 carbonaceous chondrite meteorite Allende fired into aerogel at 5 km s^{-1} could be identified and mapped from their Raman spectra. Recently, Burchell et al. (2004) have shown that complex organic materials can be fired into aerogel at 5 km s^{-1} and still be identified by their Raman signatures.

Clearly, Raman spectroscopy is a technique that works with at least some mineral and organic materials captured in aerogel at high speed. However, there are many open questions. What sort of range of mineral materials can be studied in aerogel with Raman spectroscopy? Are any important mineral species difficult or impossible to identify by Raman techniques, and what are the best operating conditions for reliable mineral identification? Do any minerals show changes in their Raman spectra as a result of the capture process? How well can different mineral components be identified in inhomogeneous particles, especially when intimately mingled? And what is the degree

of heating inherent in laser illumination during a Raman study of particles captured in aerogel? In this paper, we attempt to investigate, discuss, and resolve these issues. We have fired a wide range of minerals and inhomogeneous meteorite samples into aerogel, and we report on the Raman spectra and the effect of laser illumination on the temperature of the captured samples. All the particles in this paper that were analyzed in aerogel were captured in the aerogel at speeds typically of 4–6 km s^{-1}.

METHOD

The main tools for the work reported herein are a two-stage light gas gun (to achieve high-speed impacts in the laboratory) and two Raman spectrometer systems. The two-stage gun that was used is described in Burchell et al. (1999b). Such guns use a gunpowder charge to drive a piston. This is used to compress a light gas. The sudden release of the light gas (via rupture of a thin containing disk of metal) is used to accelerate the real projectile, which in these experiments was a mineral powder mounted in a sabot (which was discarded in flight). The speed of the shot can be selected by adjusting the amount of gunpowder, composition, and pressure of the light gas, and so forth. In flight, the projectiles travel through the range of the gun that is maintained at a low pressure of less than 1 mbar to prevent slowing of the projectiles in flight due to air resistance. The projectile used in a shot could be a single, mm-sized particle, or a number of grains of a material (typically 10 or 20 particles, each a few tens to hundreds of microns in size). The speed of the shot is found from signals given by passage of the projectiles through two laser light curtains, combined with signals from impact sensors mounted on the stop plate which intercepts the discarded sabot and the target holder. The timing information from these signals, combined with the locations of the measurement points, gives the speed in each shot, accurate to 4%.

The aerogel used in this work had a density of 60, 96, or 110 kg m^{-3}. This can be compared, for example, to the Stardust aerogels (density gradient aerogel, with a maximum density of 50 kg m^{-3}) where the cometary encounter impact speed was 6.1 km s^{-1}, compared to 4.2–6.2 km s^{-1} in this work (see below). The aerogel here was arranged in long, thin slabs (5 cm in length, 1 cm × 2 cm end face) and mounted "end-on" to provide a deep target thickness in a target holder (two or three slabs per shot). Typically, 5–10 particles per shot would hit the aerogel (i.e., 2 or 3 per slab). The tracks (Fig. 1) could easily be viewed through the side of the slabs and examined under a microscope system to show the captured particles.

The Raman system used at the University of Kent comprised a Jobin Yvon microRaman module combined with an Olympus BX40 microscope. This was coupled to a model HR640 spectrograph with liquid nitrogen cooled CCD (1024 × 256 pixels) with a 1200 gr/mm grating. The focal length of the spectrograph was 640 mm, giving a dispersion of about 0.5 cm^{-1} per pixel on the CCD (the exact dispersion varies across the spectrum), and the Raman spectra were measured with a slit width of 120 microns, although given the much stronger signal strength, the slit width was much narrower for the fluorescence spectra. Illumination was from a He-Ne laser (632.8 nm) which gave about 3 mW of power at the sample, and the measurements were made using a ×50 long working distance objective, which gave a focused laser spot of diameter ~5 μm. Accumulation time for the spectra with the Kent instrument depended on whether Raman or fluorescence spectra were being obtained. For the former, raw grains on microscope slides typically required 60–600 sec, and up to 1000 sec for grains trapped in aerogel. Fluorescence spectra were accumulated in times of less than 1 sec (raw grains on microscope slides) up to 20 sec in aerogel. All of the analyses presented herein, except those involving mapping entire grains, were performed using the Kent instrument.

Fig. 1. A typical track in aerogel (side view). An impact of rhodonite in aerogel (density 60 kg m^{-3}) at 5.1 km s^{-1}. Track length is 3.6 mm and particle size is 54 microns. The impact was from the left; the particle position is marked with an arrow.

Raman mapping of entire particles was performed at the Open University on a Jobin-Yvon LabRam HR integrated Raman microscope (focal length 800 mm) utilizing an Ar^+ ion (514 nm) laser with 7.7 mW power. The detector used was a CCD (1024 × 256 pixels) with a 600 gr/mm grating giving 3 cm^{-1} spectral resolution. The Raman spectra on this instrument were obtained from a sample volume of approximately 2 μm in diameter by 2 μm in depth by use of an LWD objective of 50 magnification. Automated X-, Y-, and Z-axis stage movement was used to raster the sample and thereby generate an array of analysis points from which spectra were obtained. The background-subtracted Raman spectrum was then manually segmented to select lines characteristic for specific mineral species, and the peak area was used to designate pixel intensity for that point in the raster, an X-Y pixel matrix thereby creating a two-

Table 1. Materials used in this Raman study.

Mineral projectiles	Idealized formula	Important extraterrestrial occurrence	Aerogel density (kg m^{-3})	Impact speed (km s^{-1})
Olivine	$(Mg,Fe)_2SiO_4$	**IDP, Ch, Pal, Mes, Ach, eCH**	96	5.1
Pyroxene (enstatite)	$MgSiO_3$	**IDP, Ach, oCh, cCh, Mes, eCH**	96	4.80
Pyroxene (diopside)	$(CaMg)SiO_3$	**oCh, cCh, Pal, Mes, Ach, eCH**	96	5.1
Serpentine (lizardite)	$Mg_3Si_2O_5(OH)_4$	**IDP, cCh**	60	5.1
Serpentine (sensu latu)	$Mg_3Si_2O_5(OH)_4$	**IDP, cCh**	110	No impacts
Feldspar (albite)	$NaAlSi_3O_8$	**oCh, cCh, Ach**	110	4.5
Nepheline	$NaAlSiO_4$	**cCh**	110	5.7
Rhodonite	$MnSiO_3$	–	60	5.1
Calcite	$CaCO_3$	**cCh**	110	4.2
Silicon carbide	SiC	**oCH, cCH, eCH, IDP, AMM**	60	6.12
Corundum	Al_2O_3	**cCh**	96	4.95
Synthetic alumina	Al_2O_3	–	110	6.2
Spinel	$MgAl_2O_4$	**IDP, oCh, cCh, Ach, eCH**	96	4.95

Key to occurrences: Ach = achondritic meteorites of howardite-eucrite-diogenite, shergottite-nakhlite-chassignite, and lunar groups; oCh = ordinary chondrites; cCh = carbonaceous chondrites, eCH = enstatite chondrites; Pal = pallasites; Mes = mesosiderites; IDP = stratospheric interplanetary dust particles; AMM = Antarctic micrometeorites. Frequent occurrences are given in bold type.

A detailed account of the distribution of these (and many other) minerals in meteorites and IDPs can be found in the chapters of Papike (ed.) 1998 and within Antarctic micrometeorites in Kurat et al. 1994.

dimensional map of mineral distribution. The accumulation time for one of these map-making scans depends on the area being scanned (i.e., how many individual point spectra are required) and can amount to periods of hours. A more detailed description is given in the section where results for these maps are presented.

MINERAL CATEGORIZATION

Previously, with the Kent Raman spectrometer, it had been shown (Burchell et al. 2001) that olivine and enstatite grains gave recognizable Raman spectra after capture in aerogel at ≈5 km s^{-1}. In addition, spinel and corundum (ruby) gave fluorescent signals that could also be used to identify those particles. In the present work, seven more minerals were investigated in addition to further study of the previous four. Details of all the minerals used are given in Table 1, along with examples of extraterrestrial materials in which they are known to occur.

The projectiles for this study were mostly chosen from a suite of homogeneous and well-characterized mineral powders stored at the Natural History Museum (NHM) in London, and previously utilized in numerous light-gas-gun shots onto glass, silicon, polymer foil, and metal surfaces. The silicon carbide powder came from a purchased artificial abrasive powder. The natural minerals for our Raman, aerogel capture, and dense substrate impact experiments were chosen from a suite of relatively coarse purchased specimens, analyzed and evaluated for absence of major compositional zonation or intergrowth with other mineral species, and subsequently catalogued into the Mineralogy Department collections of the NHM. All of the natural mineral powders were prepared by use of a pestle and ceramic mortar to crush coarser grains (typically 5 mm in diameter) selected from broken fragments of the larger specimens. While examining and selecting the coarse grains under a binocular microscope, great care was taken to avoid inclusion of other mineral species present as minor phases in the original samples. The same sieve set was used for grain-size separation for all minerals, with careful cleaning between different samples. A subsample of each mineral powder was examined in backscattered electron images, X-ray maps, and point X-ray spectra on a JEOL 5900LV analytical scanning electron microscope (SEM) with Oxford Instruments INCA energy dispersive X-ray spectrometer (EDS) at the NHM. Samples with demonstrable compositional heterogeneity (for example powders from zoned feldspars) were discarded. Analyses were also performed on a Cameca SX50 wavelength dispersive (WDS) electron microprobe at the NHM. The identity of the olivine was determined by optical microscopy of coarse green grains (~5 mm) released from oxidative breakdown of a large specimen of the Admire pallasite (BM.1950,337), the composition was determined by EDS and WDS quantitative electron probe X-ray microanalysis (EPMA) at the NHM. Mg:Fe:Mn atomic proportions were determined by WDS as 87.8:11.9:0.3, respectively, with Ca present as a trace. Minor iron oxides in irregular fractures were avoided by selection of clean, green olivine grains.

Enstatite (BM.2005,M318) from Ødegarden Mine, Bamble, Norway, was determined by optical petrographic microscopy of a polished section through a coarse pale green crystal (3 cm), and by backscattered electron imagery, EDS quantitative analysis at the NHM. Mg:Fe + Mn:Ca atomic proportions were determined as 94.8:5.1:0.1 respectively. Minor serpentine and talc veinlets were avoided in selection of material for crushing to projectile powder.

The composition and structure of Diopside (BM.2005,M310) from Yates Mine, Sandy Creek, Otter Lake, Quebec, Canada was determined by EDS quantitative EPMA. Mg:Fe + Mn:Ca atomic proportions were determined as 35.5: 15.2:49.3, respectively. Powder was prepared from 5 mm fragments broken from a cut slab of a large (4 cm) well-formed dark green crystal.

Lizardite (BM.43217) was identified by X-ray diffraction, and EDS analysis revealed almost Mg end member composition. Albite (BM.2005,M311) was prepared from a large white crystal (3 cm) intergrown with mica from Tordal, Telemark, Norway; Nepheline (BM.2005,M320) from a coarse deep red crystal (4 cm) with a thin vein of white albite on one face, from Tjolling, Larvik, Vestfold, Norway; rhodonite (BM.2005,M323) as pink chips of about 2 cm length from Broken Hill, New South Wales, Australia; calcite (BM.2005,M315) as a 4 cm transparent colorless cleavage rhomb from Creel, Sierra Tarahurama, Chihuahua, Mexico; and grains of red corundum (BM.2005,M313) and red spinel (BM.2005,M314) from a sample of coarse placer sand from Burma were all identified from compositional analyses by EDS.

The Murchison powder came from BM.1988,M.23; Allende and Orgueil from uncataloged specimens.

The choice of the specific minerals was intended to permit both assessment of appropriate analytical techniques for application to grains in aerogel (including Raman spectroscopy) and also investigation of the mineralogical effects of impact into aerogel for a wide range of mineral structures and compositions, analogous to mineral types of importance in known samples of extraterrestrial origin. From this range of materials, we were able to document the post-impact state under known velocity and target density conditions. As well as representatives of the major rock forming mafic minerals (olivine, orthopyroxenes, and clinopyroxenes), we used refractory phases such as corundum, known from refractory inclusions in carbonaceous chondrite meteorites and also from interplanetary dust particles (IDPs). Important volatile-rich phases included serpentines, known from carbonaceous chondrite meteorites, IDPs, and Antarctic micrometeorites (Kurat et al. 1994), and the calcium carbonate calcite, an important component of CM2 carbonaceous chondrite meteorites. A well-characterized feldspar (close to end-member albite composition, perhaps a little more sodic than the very common plagioclase of ordinary chondrites) provided a material with known thresholds for shock modification of structure and loss of Raman lines. Albite is also an excellent test bed for measurable volatile (Na) loss from the particle, as is nepheline, a common mineral in altered refractory inclusions within CV3 carbonaceous chondrite meteorites. Rhodonite was used in our light-gas-gun impacts to provide an easily recognized silicate composition distinct from more Fe- and Mg-rich silicates. We have thus tested a wide range of minerals found in meteoritic materials (Papike 1998 and papers therein). In each case, Raman spectra of the raw grains were obtained with the Kent Raman system.

Samples of each mineral were then fired into the aerogel of density 60–110 kg m^{-3} (aerogel densities and impact speeds as given in Table 1). Capture was successful in all cases except for the sample of serpentine (sensu latu), a hydrous phyllosilicate. Despite several attempts, no particles of this serpentine sample were found to have reached the target (i.e., no tracks were observed in the aerogel and no particle speed was obtained). It seems that the serpentine particles disintegrated under the shock of acceleration into much smaller particles, possibly of submicron size (note that the buckshot technique has proven effective in delivering less fragile grains as small as three microns onto other targets in the gun at Kent). Given the lack of tracks in aerogel, no in situ Raman work was carried out, although we note that we readily obtained Raman spectra from raw grains. However, a sample of lizardite (a serpentine group member) was successfully fired into aerogel and did give identifiable Raman spectra before and after capture. Consistent with this model of particle fragmentation is the observation that in the case of calcite some of the captured particles in the aerogel were found to be of only 5–10 microns in size, despite the fact that the initial mineral projectiles were fired as mixtures of 50 to 100 micron grains. This again suggests that substantial grain fragmentation occurred during the shot, probably as a function of the very well-developed crystal lattice cleavage that is so characteristic of this mineral. A similar fragmentation problem has also been observed in previous shots of calcium carbonate onto solar cell glass. Nevertheless, the small calcium carbonate particles in aerogel still gave recognizable carbonate Raman spectra. Separately, we note that recent experimental evidence strongly suggests that, for example, carbonate minerals (such as calcite) do not undergo substantial dissociation and loss of carbon dioxide even at the peak shock pressures experienced during hypervelocity impact (Jones et al. 2000).

In situ Raman or fluorescence spectra, sufficient for mineral identification, were obtained with the Kent Raman system for all the minerals captured in the aerogel. Typically, spectra were obtained from four or five raw grains and a similar number of grains in aerogel. The Raman spectra for the raw grains and for the grains trapped in aerogel are shown as pairs for comparison in Fig. 2 and are clearly similar. Although this figure shows some of the best matches between the grains before shooting and after impact in aerogel, these are typical of the majority of spectra, with only small variations in relative peak heights from spectrum to spectrum. It is notable that many of our Raman spectra were obtained from depths into the aerogel of between 5 mm and a maximum of about 1 cm of aerogel, with no signal/noise problems at these depths. Thus, for a wide range of minerals, the capture process in aerogel at velocities comparable to

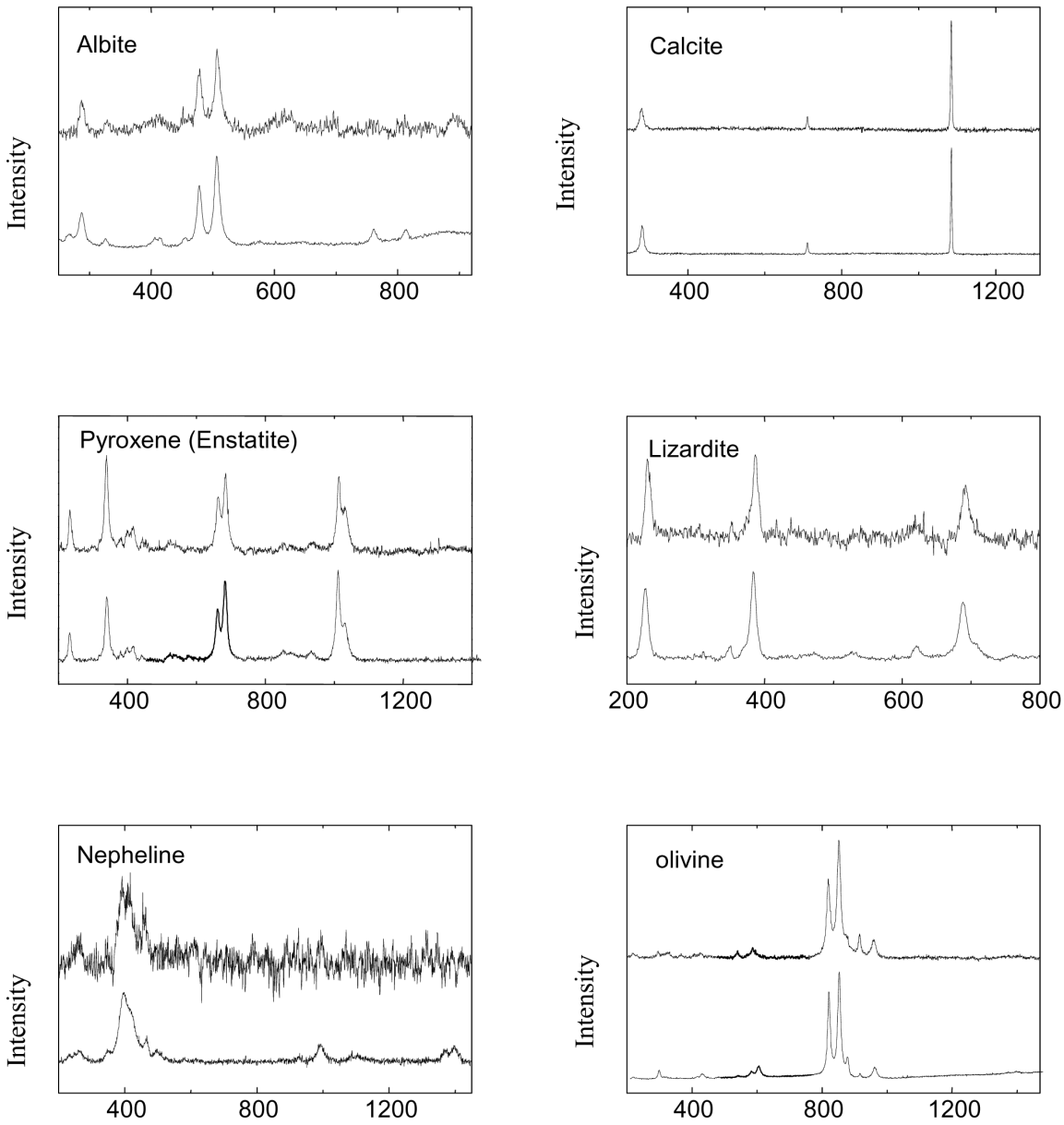

Fig. 2. Raman spectra of mineral grains, showing in each case the spectrum of a grain trapped in aerogel (upper trace) and the spectrum of a raw grain from the same mineral sample (lower trace). See Table 1 for aerogel density and impact speed.

those of the Stardust/Comet Wild-2 encounter has neither obscured nor so significantly altered the spectra as to make them unrecognizable. Indeed, the spectra from impacted grains of albite feldspar retain the Raman lines characteristic of the original mineral, in contrast to the loss of fine peak structure seen in Raman spectra we have observed from masculinity (shocked, isotropic feldspar) in the basaltic shergottite meteorite Los Angeles 001, and in shocked basaltic clasts from the melt-rich impactites of the Lonar impact crater in India (unpublished work). It is particularly significant that such important information can be obtained from impacts into aerogel of relatively high density (110 kg m^{-3}), and encouraging for survival of material impacting into lower density aerogel such as that on the Stardust spacecraft (20 kg m^{-3}).

Silicon carbide was also examined as part of this study because grains of this composition have been reported in primitive unequilibrated chondritic meteorites (Bernatowicz et al. 1987), and are survivors from the proto-solar nebula. They can also be present as individual discrete grains among the population of interstellar dust particles (ISP). Presolar SiC grains carry trace element isotopic signatures that demonstrate their environment of origin and are characteristic of specific nucleosynthetic processes (e.g., Zinner 1998;

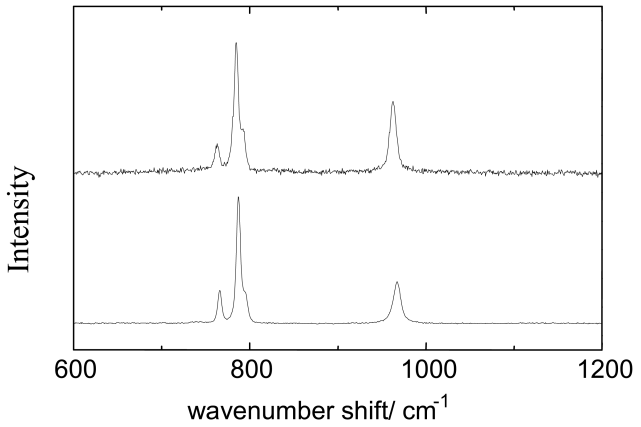

Fig. 3. Raman spectra of a silicon carbide grain in aerogel (top spectrum), and of a raw silicon carbide grain (bottom spectrum). See Table 1 for aerogel density and impact speed.

Amari et al. 2001). They may be vulnerable to destruction through oxidation during many processes of meteoritic equilibration at elevated temperatures and in the presence of reactive volatiles. It is not yet known whether silicon carbide is present within cometary particles, although the postulated lack of post-nebular alteration events in smaller icy bodies (a few km in diameter) accreted outside 20 AU may suggest their likely survival. Using silicon carbide, shots into aerogel were carried out at 5 km s^{-1}. Unlike the other materials in Table 1, the Raman spectra of individual SiC grains showed significant variations in the structures and relative intensities of the main bands. These variations are well known to be mainly due to polymorphism in SiC (Nakashima et al. 1986). In seeking a match between the spectra of captured SiC particles and raw SiC grains, it was therefore necessary to select from several raw grain spectra. The Raman spectrum (obtained with the Kent system) from a typical SiC particle taken in situ after capture in aerogel and a matching raw grain spectrum are shown in Fig. 3. The recognition of SiC grains within undisturbed aerogel by a relatively noninvasive and contamination-free technique is potentially very important. It will allow location of individual grains and their careful physical preparation, using techniques such as those of Westphal et al. (2002, 2003) prior to trace element isotopic analysis without grain damage or contamination.

The majority of projectiles investigated in our study were of single mineral crystals, or were relatively strong fragments of carbonaceous chondrite meteorite (see below), both of which may penetrate aerogel deeply, leaving an obvious discrete particle remnant near the terminal point of the track. It is possible that delicate "fluffy" particles, which appear in interplanetary dust collections and which may dominate fresh cometary dust (Bradley and Brownlee 1986; Greenberg and Hage 1990), will be even more prone to disintegration during capture. Such capture events will probably result in aerogel tracks, which may contain micron-sized (or smaller) debris

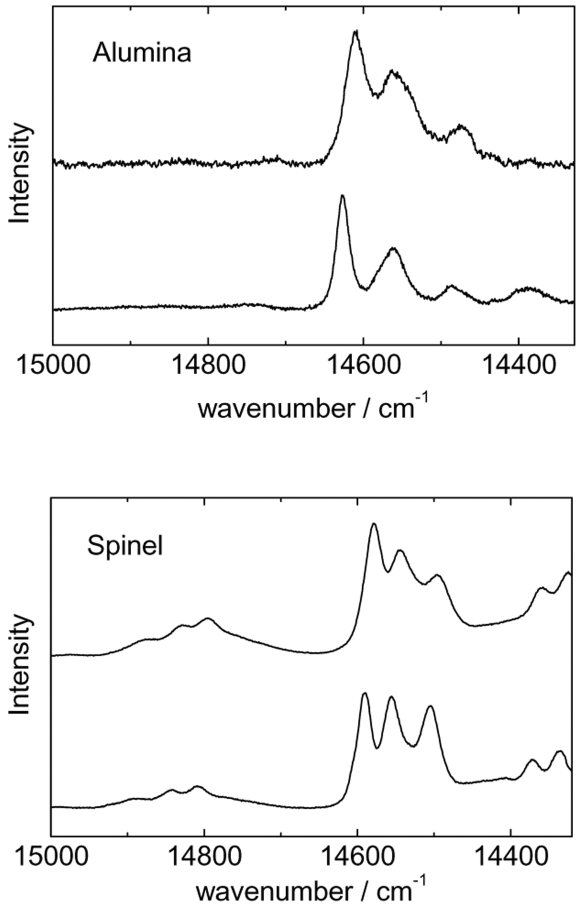

Fig. 4. Fluorescence spectra of alumina and spinel (raw grains and grains trapped in aerogel) excited by the helium neon laser. In each case, the lower trace is the raw grain spectrum and the upper trace is from the grain captured in the aerogel. The spectral range shown corresponds to wave number shifts of 803 to 1475 cm^{-1} from the 632.8 nm laser line. See Table 1 for aerogel density and impact speed.

along the track rather than a relatively large captured grain at the end. In such cases, a Raman analysis of the debris along the length of a track should be attempted as well as of any fragment at the end of a track. Raman techniques may work on submicron-sized objects, although the smallest objects identified here were approximately 3 microns across.

In addition to the minerals in Table 1 characterized by their Raman spectra, two other materials of extraterrestrial significance, corundum (alumina) and spinel, gave distinctive spectra, but due to fluorescence rather than Raman scattering. Fluorescence was attributed to Cr^{3+} ions, an important minor component of the corundum samples. As with the Raman spectra, the fluorescence spectra shown in Fig. 4 are sufficiently distinctive to be of fingerprint value for recognizing these substances (Note that, as stated earlier and as is conventional for emission spectra, the fluorescence spectra in Figs. 4, 5, and 11 are shown with an absolute wave number scale, rather than with a wave number shift scale as is

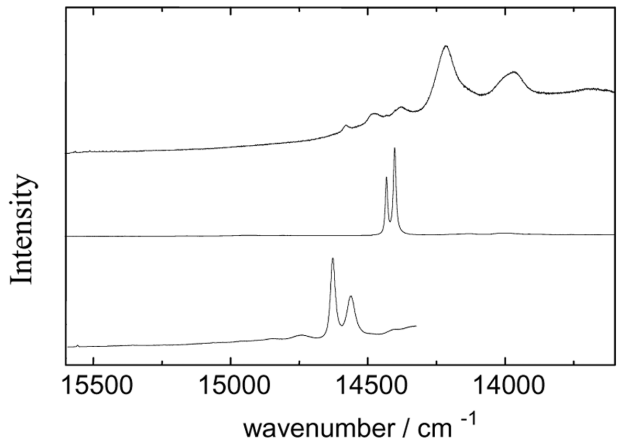

Fig. 5. Three distinct fluorescence spectra observed from alumina samples, excited by the helium neon laser. The lowermost spectrum is the one most commonly found in our samples. The spectral range shown corresponds to wave number shift of 200 to 2200 cm^{-1} from the 632.8 nm laser line.

conventional for Raman spectra). Alumina is of interest since fine aluminium powder is a major component of solid rocket motor fuel and produces small Al_2O_3 particles in the rocket's exhaust. Thus large numbers of micron-sized alumina particles are regularly injected into Earth orbit from spacecraft rocket engines and can be expected to feature in any aerogel sample exposed in Earth orbit. Although the alumina powder used in our shots was from a single source of synthetic alumina, an examination of the raw grains and those in the aerogel (density 110 kg m^{-3}, impact speed 6.2 km s^{-1}) also found evidence for some grains with different fluorescent spectra. These are shown in Fig. 5 (where the lower spectrum is the one most commonly found, and the upper two are the variants). No explanation was found for this diversity in the single source of alumina, but major differences in color of natural corundum grains can be explained by minor variation in the content of first row transition elements. Similarly, in the case of the spinel samples, thought to be a homogeneous sample of natural red spinel grains from an alluvial placer deposit, distinct fluorescence spectra revealed two quite different grains, one with characteristic ruby fluorescence. Detailed compositional analysis of grains in a sample of the projectile powder showed that prior to mineral crushing and sieving, some ruby grains (a red form of natural corundum, impure alumina) had been mistaken for red spinels, and incorporated into the sample, and had contaminated an otherwise homogeneous mineral sample. The standard spectra for corundum (alumina) and spinel are those shown in Fig. 4. The distinction between these two materials was also clear after their capture in aerogel.

It thus seems clear from the minerals studied that the potential for use of Raman analysis after hypervelocity capture in aerogel is not limited to just a few minerals. Indeed, all the materials successfully fired into aerogel gave recognizable signals afterward (either Raman shift spectra or fluorescent spectra). It is clear that this type of analysis can be used to search for a wide range of interesting materials captured in aerogel.

METEORITE SAMPLES

Having demonstrated that hypervelocity capture in aerogel is not a priori destructive of the characteristic Raman signal from minerals, the next step in the work was to investigate capture in aerogel of particles of mixed composition and to attempt to identify their compositions using Raman techniques. Since study of extraterrestrial materials is the purpose of dust collection in space, meteoritic samples were used as analogues of one likely major source of interplanetary dust, for example Main Belt asteroids of the spectroscopic C-type (Gaffey 1999). The meteorite samples chosen were the carbonaceous chondrites: Orgueil (CI, type 1, dominated by hydrous phyllosilicates, iron sulfide and iron oxide grains); Murchison (CM, type 2, with a fine-grained matrix bearing hydrous phyllosilicates and with well-defined chondrules dominated by anhydrous mafic silicates, olivine, and pyroxene) and Allende (CV, type 3 oxidized, with a fine-grained anhydrous silicate matrix, abundant mafic silicate chondrules, and refractory inclusions rich in aluminium and calcium). Each meteorite is well-documented and is demonstrably inhomogeneous in composition at the scale of a few micrometers.

The extensive literature on the structure, mineralogy, and composition of small extraterrestrial particles collected in the stratosphere (e.g., the review by Rietmeijer 1998) shows that silicate minerals similar to the olivines, pyroxenes, sulfides, and the layer silicates found in the carbonaceous chondrite meteorites listed above are major constituents of many interplanetary dust particles (IDPs). Although the relative proportion of IDPs that come from asteroidal sources is still a matter of debate, there is general consensus that many are likely to be of cometary origin. Anhydrous silicates have been positively identified by remote sensing observations of the cometary environment (Crovisier et al. 1997), and these minerals might therefore be expected to occur in samples of dust collected directly from a comet by a mission such as Stardust. However, many IDPs contain amorphous, noncrystalline silicate and carbonaceous materials, perhaps the result of prolonged energetic irradiation in space (Bradley 2003, 2004) and it is possible that such materials may not yield a distinctive Raman or fluorescence signature. Nevertheless, we believe that Raman spectroscopy of grains embedded in aerogel from the Stardust encounter with comet Wild-2 should provide an important link to the distinctive mineralogy of small particles collected in the stratosphere and micrometeorites from Antarctic ice (Kurat et al. 1994).

This work proceeded in two phases (using the Kent Raman system). Firstly, several raw grains of each meteorite

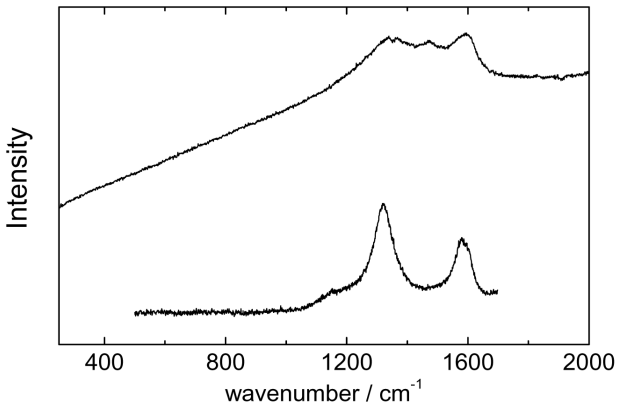

Fig. 6. Spectra showing (upper trace) Raman bands due to highly amorphous carbon in raw Murchison meteorite grains superimposed on a rising background due to sample fluorescence, and (lower trace) less broad Raman bands indicative of less disordered carbon, with a structure closer to that of graphite, in Allende meteorite grains.

were studied providing 10–20 spectra per meteorite. Spectra that only displayed the peaks characteristic of the presence of carbon (e.g., Fig. 6, broad peaks at 1350 and 1594 cm^{-1}) were discarded and the remaining spectra were first compared for matches to those we obtained for the standard terrestrial minerals in Table 1, and then the remainder were compared with the Raman spectra of minerals available on a database of Raman spectra (http://minerals.gps.caltech.edu/FILES/raman/Index.htm and links therein). Note that in doing this latter comparison, we make the assumption that since all the materials tested so far yielded similar Raman spectra before and after capture in aerogel, it was taken that this was true for all minerals with high dissociation temperatures. There is no proof of this, but in the circumstances, it is a useful and not unreasonable assertion. Matches were found that indicated the presence in the meteorite samples of the minerals listed in Table 2, and only one of the spectra remained unmatched after this process. Examples showing the matches to spectra of our standard mineral samples are given in Fig. 7. The minerals detected include olivine, enstatite, albite, calcic clinopyroxene, sulfur, haematite, and the titanium dioxide anatase, with the additional presence of amorphous carbon in some of the grains, as indicated by the superimposed broad peaks at 1350 and 1594 cm^{-1}. Only in one or two cases was the match ambiguous. Thus one spectrum could have been either dolomite or magnesite, which are closely related magnesium-bearing carbonate minerals, both known from carbonaceous chondrite meteorites. Another spectrum contained bands characteristic of sulfate ions superimposed on bands indicative of sulphur. On comparing with standard spectra available to us, these sulfate bands gave a better match to jarosite than to simple sulfates such as barite or anhydrite, though it is likely that there are other sulfate-containing minerals that would have given a similar match. In any case, caution is required before assigning the identified minerals as being part of the primordial body. For example, the presence of sulphur is anomalous and may be related to the growth of sulfates within the meteorite, which is known to occur rapidly after arrival on Earth (Gounelle and Zolensky 2001) and possibly their reduction by microbial processes. From these results, it is clear that Raman techniques can be used to identify individual mineral grains in meteorite samples, confirming previous work (e.g., see Popp et al. (2002) for a recent paper on the subject).

Table 2. Minerals successfully identified by Raman spectra of raw meteorite grains.

Meteorite	Composition from Raman spectra
Murchison	Magnesite/dolomite
	Olivine
	Anatase
	Enstatite
Orgueil	Barite
	Jarosite
	Sulfur
	Epsomite
	Hematite
	Albite
Allende	Olivine
	Diopside (pyroxene)

As the second part of the experiment, samples of each meteorite were fired into aerogel (Murchison with aerogel density 96 kg m^{-3} and impact speed 5.20 km s^{-1}; Orgueil with aerogel density 96 kg m^{-3} and impact speed 5.56 km s^{-1}; Allende with aerogel density 110 kg m^{-3} and impact speed 5.58 km s^{-1}). Despite attempts to obtain good-quality Raman spectra from six grains, no strong spectra were obtained from the Murchison samples. The best spectra showed possible olivine peaks and the bands indicative of the presence of carbon. By contrast, good spectra were obtained from specific locations on the captured grains of Allende and Orgueil (examples are shown in Fig. 8, displaying clear Raman lines attributable to olivine and pyroxene within the meteorites).

Finally, using the higher spatial resolution and the mapping capability of the Open University LabRam spectrometer, Raman maps of a depth-resolved slice through an entire Allende grain were also generated. This was achieved using the rastering method (also see Graham et al. 2001b), with rapid point sampling (typically 6 seconds for a complete spectrum acquisition at each pixel point). At each pixel point, a full spectrum was collected (typically from 0 to 2500 cm^{-1} shift) and stored as a pristine data set for further analysis after the map completion. To produce maps from the raw data set, a range of spectrum background fitting and subtraction methods were used. Individual pixel spectra, or the sum of all the spectra, were used to define wave number bounds between which the signal level was integrated to yield an intensity measurement. For each defined segment of the spectrum, a grayscale image of Raman line intensity was

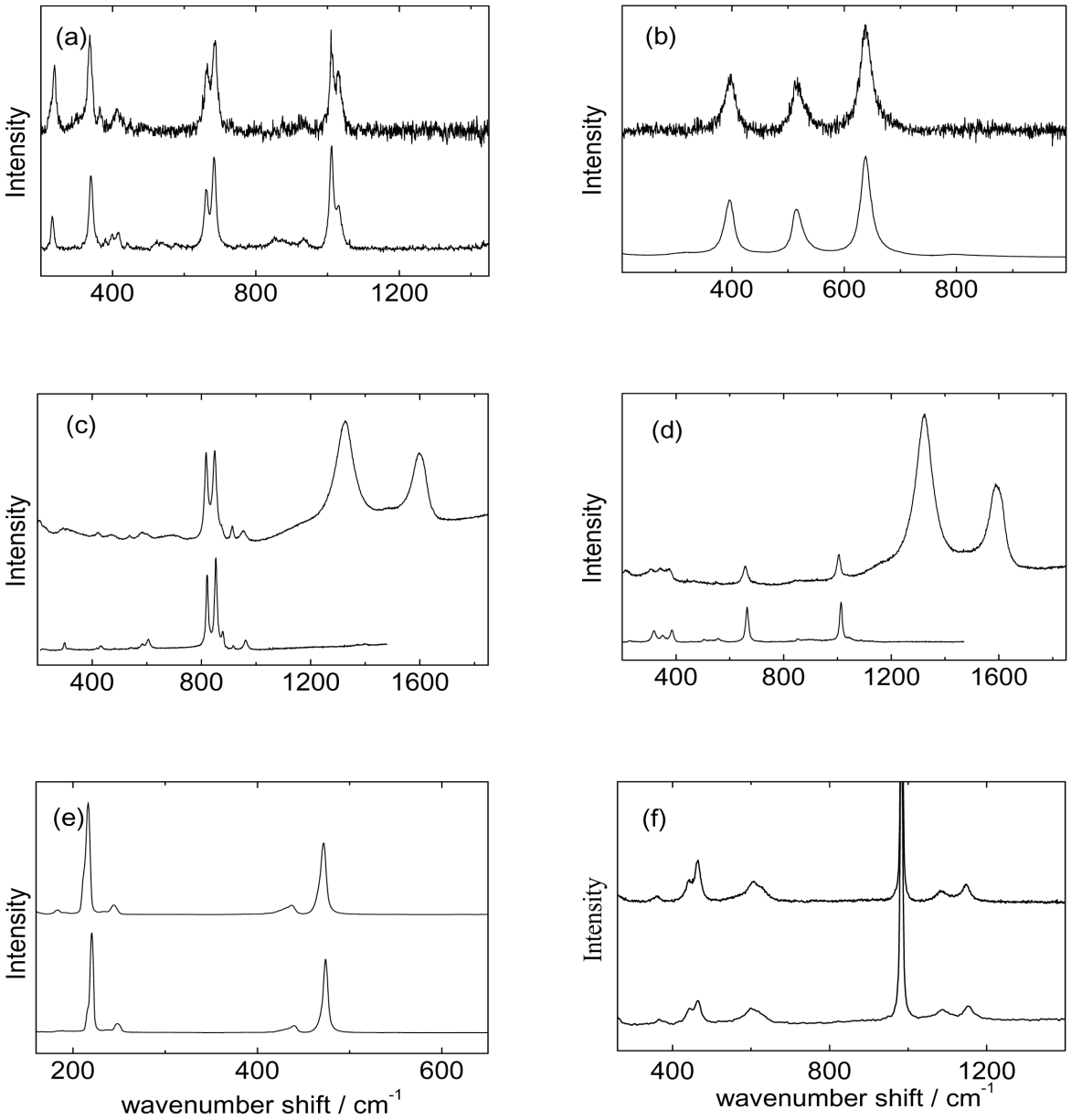

Fig. 7. Raman spectra from raw meteorite samples (upper trace in each plot) matched with the spectra of standard mineral samples (lower trace). a) and b) Murchison meteorite showing a match for enstatite and anatase; c) and d) Allende showing a match for olivine and pyroxene; e) and f) Orgueil showing a match for sulphur and epsomite. The Allende meteorite spectra also show the presence of graphitic carbon (see Fig. 6).

generated, as shown in Fig. 9. Thus the entire volume of a semi-transparent grain encapsulated within aerogel can be analyzed and a map of mineral locations produced. Examples of maps from a grain of the Allende sample captured in aerogel are given in Fig. 9. A green (514.5 nm) laser was used with 7.7 mW output, and the Raman signal was acquired through a ×20 objective. In Figs. 9b and 9c, the characteristic peaks at 817 and 851 cm^{-1} were chosen to indicate the location of olivine. The differing intensities for the two lines are a function of the differing crystallographic lattice orientations in the two grains, generating polarization contrast in the Raman line expression. In Fig. 9d, 1590 cm^{-1} was chosen, indicative of the presence of carbon, demonstrating that this impacted grain contains both undamaged silicate minerals and probably original meteoritic organic matter. The size of the grain (see in white light in Fig. 9a) was 60 microns across, and the spot size (i.e., minimum potential spatial resolution in these maps) was approximately 3 microns.

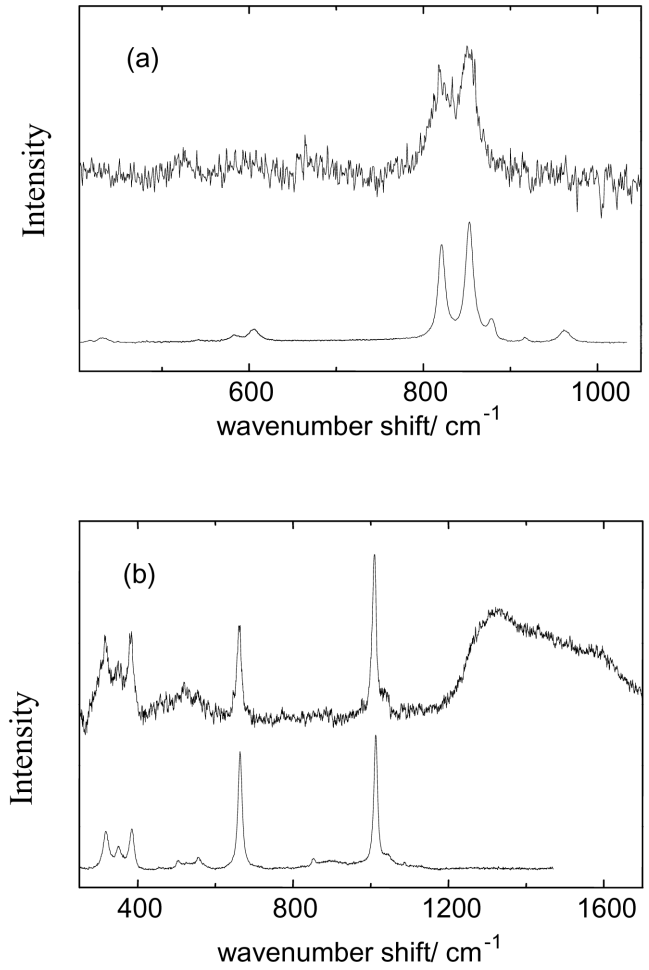

Fig. 8. a) Raman spectrum (upper trace) from Allende meteorite sample captured in aerogel (density 110 kg mm^{-3}) at 5.58 km s^{-1}, and (lower trace) a reference spectrum of olivine; b) Raman spectrum (upper trace) from Orgueil meteorite sample captured in aerogel (density 96 kg mm^{-3}) at 5.56 km s^{-1}, and (lower trace) a reference spectrum of pyroxene. In (b), the broad band at 1300–1600 cm^{-1} in the upper spectrum of indicates the presence also of amorphous carbon in the captured Orgueil particle.

HEATING OF SAMPLES

Aerogel is an extremely poor thermal conductor (as low as 0.01 W m^{-1} K^{-1} for very low density aerogels), and one of the open issues with regard to use of Raman techniques on particles trapped in aerogel concerns the possibility of grain heating by the laser and consequent structural and chemical changes in the samples. The degree of heating of small grains during Raman analysis has therefore been investigated using the Raman spectrometer at the University of Kent. In this spectrometer, the laser beam (3 mW at the sample) is focused into a spot size of ~5 μm diameter, giving a power density of about 150 W mm^{-2}, and thus in a highly insulating medium such as aerogel there is likely to be significant heating of particles which absorb at the laser wavelength.

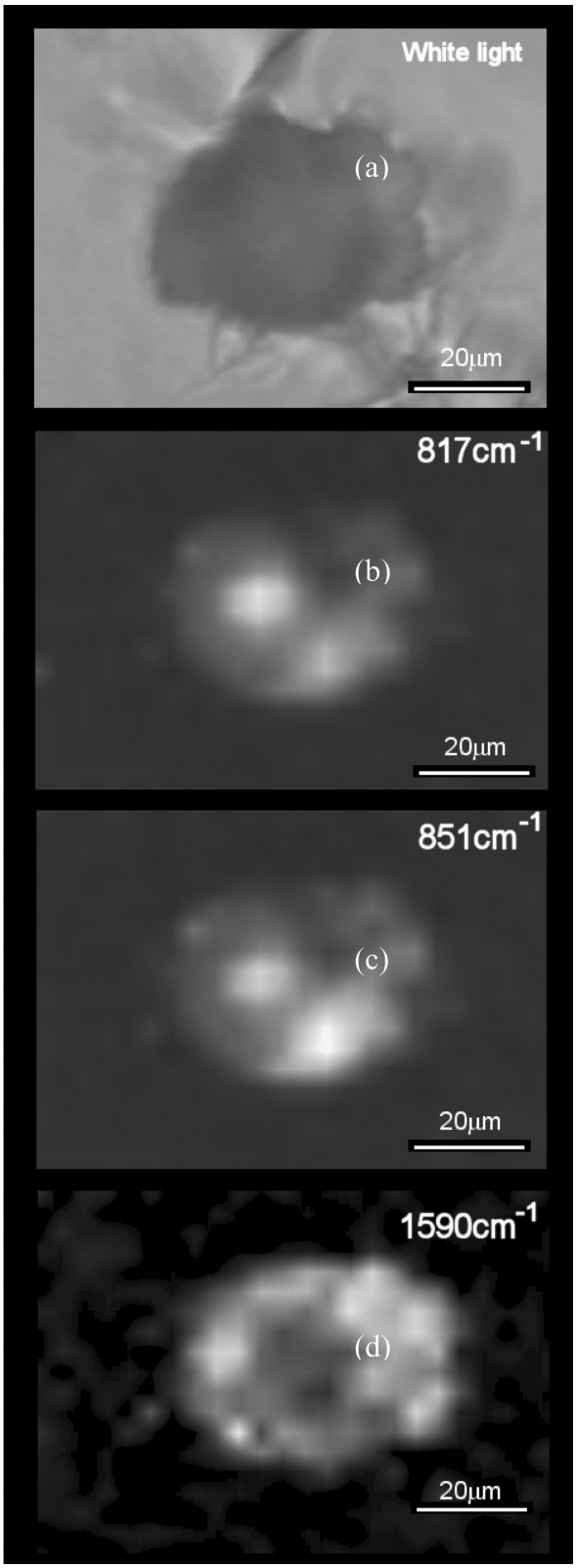

Fig. 9. Allende grain in aerogel (density 110 kg mm^{-3}, impact speed 5.58 km s^{-1}). a) white light illumination, and Raman maps at (b) 817 cm^{-1} (i.e., olivine), c) 851 cm^{-1}, (i.e., olivine), and d) 1590 cm^{-1} (i.e., indicative of carbon).

Information on sample temperature has come from three types of measurement. First, use has been made of the relative intensity of corresponding Raman bands on the low and high frequency sides (the Stokes and anti-Stokes sides) of the laser line. This intensity ratio is given by

$$R = \frac{I_{Antistokes}}{I_{Stokes}} = \left(\frac{v_0 + v}{v_0 - v}\right)^4 \exp\left(\frac{-hvc}{kT}\right)$$

where v_0 is the wave number of the incident light from the laser, v is wave number shift for a particular Raman band, h is Planck's constant, c is the speed of light, k is Boltzmann's constant, and T is the temperature. From the measured ratio R, the temperature can therefore be obtained.

Raman bands on the anti-Stokes side were found to have fairly poor signal/noise ratio, particularly at large shifts from the laser line, and it was important that a curve-fitting package was used to measure the peak heights. Use was made of the package Peaksolve (Galactic Industries), and the bands were fitted to a mixed Gaussian Lorentzian or a Voigt band shape. It was also necessary to multiply the measured intensity ratios R by a correction factor to correct for the variation in spectrometer sensitivity across the spectrum. This factor was determined from measurements of R for several bands of the colorless liquids acetone, bromobenzene, tetrachloromethane, and toluene. Since these liquids do not absorb at the laser wavelength, the correct value of the ratio R for each band could be calculated from the equation above with T set equal to room temperature. The correction factor at the wave number of each band of these liquids was then the ratio of the calculated and measured values of R. The numerical value of this correction factor, which varied smoothly over the spectral range of interest, was 0.78 for Raman bands on the Stokes and anti-Stokes side of the laser line with shifts of 400 cm^{-1}, and 1.02 for Raman bands with shifts of 1000 cm^{-1}. Because of the difficulty of measuring the intensities of weak bands in the presence of noise, particularly on the anti-Stokes side, there was some spread in the temperatures obtained from different bands in the same spectrum, or from repeat scans. From this spread, the limits of accuracy of this method were estimated to be ±20° near room temperature, and ±60° near 500 °C.

Stokes/anti-Stokes Raman measurements were first carried out on various small (10–50 μm) particles in air on a microscope slide, and these showed that even in air there was significant heating of strongly absorbing particles. Thus for silicon carbide particles, which in bulk were dark gray, the temperature ranged from room temperature to 160 °C, with most of the particles in the range 100–160 °C. Olivine and calcite particles, however, which have low absorption at the laser wavelength, were found to be at room temperature within experimental error. The temperatures of particles of these substances in aerogel were found to be somewhat higher, typically respectively 180 (silicon carbide, Fig. 10a), 20 (olivine), and 60 (calcite) °C, at this laser power. However

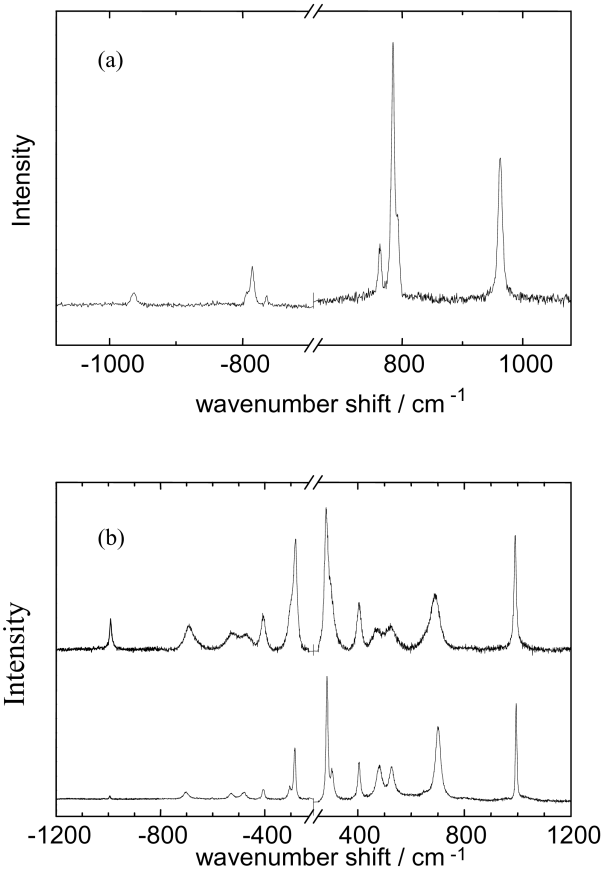

Fig. 10. a) The Stokes and anti-Stokes Raman lines for a silicon carbide particle trapped in aerogel, T = 180 °C. b) Raman spectra of a strongly absorbing particle (size 50 μm) trapped in aerogel on both the anti-Stokes and Stokes sides of the laser line, showing (upper trace) the effects of laser heating of the sample. The upper trace shows a spectrum recorded with a laser power of 2 mW at the sample, and the lower trace shows an identical run except that the laser power was reduced to 0.2 mW. Of note are the much weaker bands on the anti-Stokes side in the lower trace, indicating the lower sample temperature. See Table 1 for aerogel density and impact speed.

a much higher temperature was recorded for a particle of an unknown impurity in the silicon carbide sample shot into the aerogel, which reached 480 °C (Fig. 10b, upper trace) in the focused laser beam. The Raman spectrum of this particle with the laser attenuated to 10% of full power (giving a temperature calculated from the Stokes/anti-Stokes ratio of 75 °C) is also shown in Fig. 10b (lower trace). It can be seen that not only are the bands on the anti-Stokes side more intense in the spectrum at the higher laser power, but also the band widths are much greater at the higher power, clearly confirming the large difference in sample temperatures at the two laser powers. This illustrates how control of the laser intensity can significantly change the temperature achieved by the illuminated particle. Thus in all Raman measurements on particles trapped in aerogel, the basic principle should be to use the lowest illumination required to extract a spectrum. In this context, it should be noted that heating to an

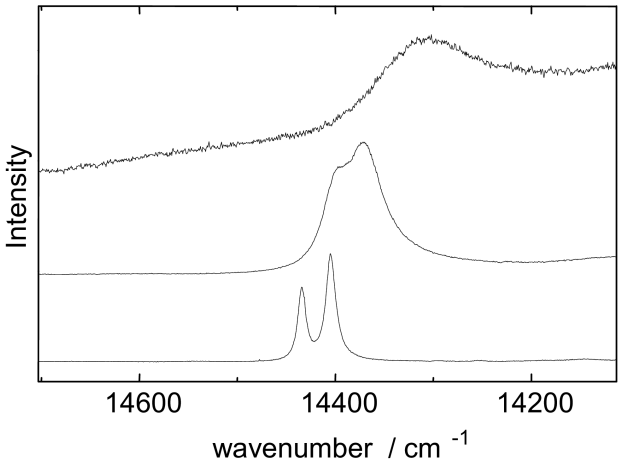

Fig. 11. Fluorescence spectra from a corundum particle in aerogel at 3 mW laser power (top spectrum), and (middle and lower spectra) with the laser beam attenuated to approximately 50% and 0.1% of full power, respectively. The spectra have been scaled and shifted vertically for ease of comparison. See Table 1 for aerogel density and impact speed.

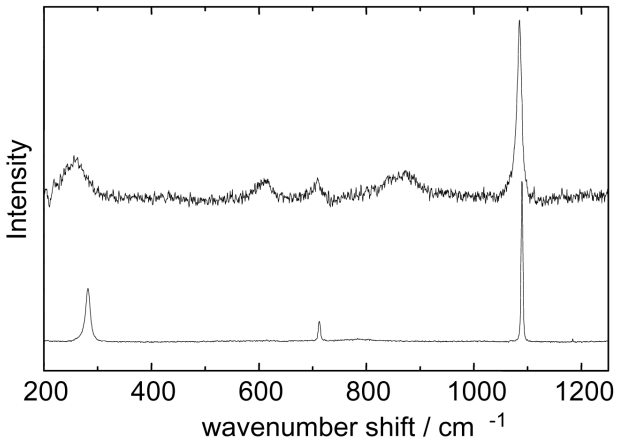

Fig. 12. The top spectrum shows a calcite particle in aerogel, showing band shifts and broadening consistent with laser heating to ~600 °C. The bottom spectrum shows calcite at room temperature. See Table 1 for aerogel density and impact speed.

equilibrium temperature occurs rapidly on time scales less than 1 sec, and so for normal Raman integration times the magnitude of the heating depends on the power delivered rather than the duration of the illumination.

The second method that has been used to estimate the temperature of particles at the laser focus makes use of the fluorescence excited in ruby particles by the helium neon laser. This fluorescence consists of a pair of sharp emission bands near 14,400 cm^{-1}, which thus lie in the same spectral region as Raman bands excited by the helium neon laser and are therefore readily recorded using the Raman spectrometer. The wave numbers of these bands are well known to be dependent on temperature and pressure, and they have been much used for the measurement of pressure in high-pressure cells. The wave numbers of these bands vary approximately linearly with temperature near 300 K with gradient –0.14 cm^{-1} K^{-1}, and this variation has been presented graphically over the range 50 to 800 K (McCumber and Sturge 963). Interpolation of the measured fluorescence shifts in the published graphical data thus gives the temperature of ruby particles at the laser focus. Although confined to ruby particles, this method is of much greater accuracy for small changes in temperature than that based on Raman Stokes/ anti-Stokes intensity ratios because of the greater accuracy of measurements of band wave number than band intensity. It was estimated that below 150 °C where the fluorescence bands have a full at half height of less than 30 cm^{-1} with very low noise, the band centres in the spectra could be measured to 0.5 cm^{-1} by fitting a mixed Gaussian Lorenzian bandshape to the fluorescence bands, giving a temperature accuracy of ±4°. This accuracy is reduced above 150 °C because of broadening of the fluorescence bands at higher temperatures.

Fluorescence measurements were first made on roughly 30 ruby particles in each of the size ranges ~50 μm and 5–10 μm in air on a microscope slide. The particles were of natural mineral origin, and are therefore not expected to be homogeneous in composition, and thus in their optical absorbance at the laser wavelength. Considerable variation on the temperatures of individual ruby particles in the focused laser beam was therefore expected. In fact no shift from the room temperature fluorescence wave number was found for any of the larger particles, or for well over half of smaller particles, and for ca. 20% of the smaller particles the shifts were 5 cm^{-1} or less (temperatures in the range 20 to 56 °C). For one particle (8 μm diam.) in air, however, the shift was 55 cm^{-1}, corresponding to a temperature of 395 °C. When examined after being fired into aerogel, much larger heating effects were apparent, and thus of 15 ruby particles examined in aerogel almost all showed shifts in the fluorescence, giving temperatures fairly evenly distributed over the range 20 to 230 °C. However one particle of dimensions about 25 μm had a fluorescence shift of 96 cm^{-1}, showing that this particle was heated by the laser to ~700 °C. The fluorescence of this particle at the full laser power and at lower powers is shown in Fig. 11. This clearly shows the expected change in temperature as the laser power is varied, thus leaving beyond doubt that the fluorescence shifts are due to laser heating. Also of note is the sloping baseline which appears in the spectrum at full laser power, due to the black body emission of the particle at 700 °C.

It is clear from these observations that the extent of laser heating does indeed vary considerably for different particles, and is greater for particles in aerogel than in air. However, it is important to note that for the majority of samples in aerogel whose temperatures we have measured, temperatures did not exceed 200 °C. Thus for many mineral particles in

aerogel at laser power densities comparable to our spectrometer, laser heating is likely to be insufficient to cause significant change.

Where temperatures above 200 °C were observed, this seems to correlate with high absorption at the laser wavelength and with small particle size. The large differences in laser heating among silicon carbide and ruby particles mentioned above are almost certainly related to variations in the amount of laser absorption, due to differences both in their dimensions and in the optical absorbance of individual particles. More surprising, however, is a calcite particle fired into aerogel whose Raman spectrum is shown in Fig. 12. The Raman spectra of the other calcite particles that have been examined in aerogel are those of calcite at room temperature (see Fig. 2, for example) as expected since calcite is non-absorbing at the laser wavelength. But for this anomalous particle, the spectrum is that of calcite at a much high temperature, showing the band broadening and shifts to lower wave numbers (particularly of the lattice vibration near 280 cm^{-1}) that have been reported previously as characteristic of calcite at a high temperature (Gillet et al. 1993). The work of Gillet et al. gives the variation of the wave numbers of the calcite bands over the range 20 °C to just below the decomposition temperature of calcite near 800 °C, and interpolation of the calcite wave numbers in these data provides a third method for investigating laser heating of Raman samples. Using the notation of Gillet et al. to label the calcite bands, our experimental wave numbers for the anomalous calcite particle and (in brackets) for a room temperature calcite sample are A_{1g} (ν1), 1084.9 (1089.6) cm^{-1}; E_g (ν4), 709.6 (712.5) cm^{-1}; E_g (lattice), 258.2 (281.9) cm^{-1}. From these data the temperature of the anomalous trapped calcite particle is estimated to be about 600 °C. The band widths of the 1084.9 and 258.2 cm^{-1} bands at 600 °C interpolated from the graphical data on bandwidth versus temperature in the Gillet et al. paper are respectively 11 and 52 cm^{-1}. These are to be compared with the measured bandwidths of 9 and 51 cm^{-1} for the anomalous trapped calcite particle (Fig. 12, upper trace), thus supporting the 600 °C temperature. The bandwidths for the 1089.6 and 281.9 cm^{-1} bands of room temperature calcite (Fig. 12, lower trace) are respectively 4 and 10 cm^{-1}. This high temperature of the anomalous calcite particle in aerogel is consistent with the temperatures of some of the other trapped particles reported above. It is, however, a surprising result, since pure calcite is colorless and is therefore not expected to absorb the light from the laser. It thus seems likely that, in this case, there is the additional presence of other strongly absorbing material in this trapped particle.

Of relevance to these temperature measurements are our experiments on volatile-rich, hydrous materials such the phyllosilicate serpentine (sensu latu sample), raw grains of which on microscope slides have shown no apparent change in the Raman spectral properties when subjected to intense green laser irradiation for intervals as long as 2 hours. As the thermal decomposition of serpentine is well understood from experimental data, and occurs with the loss of water and creation of anhydrous silicates such as olivine at a temperature of 500 °C, it seems that this temperature was not reached during laser irradiation of those samples. It is unfortunate that not all the serpentine samples survived acceleration in the light gas gun, so were not all captured in aerogel. The capture process may alter the grains, so this is a critical point for further study. We also suggest that in situ heating due to the laser illumination during Raman analysis combined with the poor heat conduction properties of the aerogel may be a critical source of heating for phyllosilicates. In this study, one sample generically labelled serpentine (sensu latu) did not survive acceleration despite several attempts, but a sample of Lizardite (a member of the Serpentine group) did and provided Raman spectra both before and after capture in aerogel. Although not done here, even if launch of serpentine in a light gas gun is not possible for all group members, it should be possible to insert grains into aerogel by hand and then to conduct a Raman analysis. This is left for future work and would at least test for possible deleterious effects of Raman analysis conducted in situ in aerogel, although it will not address the issue of whether the capture process itself alters the mineral.

CONCLUSIONS

There are a variety of appropriate techniques for study of small extraterrestrial particles (see Zolensky et al. 2000). Our extensive study of Raman techniques (first demonstrated by Burchell et al. 2001) shows them to be successful in identifying a wide range of minerals after their capture in aerogel at speeds of 5 to 6 km s^{-1}. In some cases, fluorescence spectra have been obtained which are similarly useful in aiding identification. It is clear that success is not limited to just a few mineral types, but encompasses a wide range, and includes many of interest to planetary science. The laser illumination spot size can be small (of the order of 5 microns across) with useful information gained from particles of similar or even smaller size. This suggests that Raman spectral techniques are well-suited to the size range of the coarser particles expected to be found in the Stardust aerogels. Further, it has been demonstrated that Raman mapping of particles containing a diverse suite of minerals (e.g., small grains of the Allende and Orgueil meteorites) can be carried out in situ in the aerogel. This has potential as a sensitive tool for characterization of particles comparable in size to IDPs and Antarctic micrometeorites, although not all samples (e.g., our grains of Murchison) give strong signals.

In addition, a study has been carried out of the heating effects on particles in aerogel during the laser illumination necessary for Raman study. Elevated temperatures were

obtained for some of the particles in aerogel, but in the main, usable Raman spectra could be obtained with modest elevations in temperatures. Caution is thus advised and this suggests use of the lowest laser power on the sample that is compatible with obtaining a Raman spectrum.

Overall, Raman spectroscopy is increasingly emerging as a powerful tool for study of extraterrestrial samples captured in aerogel. The return to Earth of the Stardust mission aerogel in 2006 will be keenly awaited. The 2800 ± 500 particles bigger than 15 microns that are predicted to have impacted that aerogel (Tuzzolino et al. 2004) at 6.1 km s^{-1} will be an invaluable resource for analysis. Provided intact particles exist at the ends of tracks, or fragments of greater than a few microns line the track walls, the material will be suitable for study by Raman techniques.

Acknowledgments–We thank M. Cole for the firing of the light gas gun and the Particle Physics and Astronomy Research Council (UK) for financial support.

Editorial Handling—Dr. Scott Sandford

REFERENCES

Amari S., Nittler L. R., Zinner E., Gallino R., Lugaro M., and Lewis R. S. 2001. Presolar SiC grains of type Y: Origin from low-metallicity asymptotic giant branch stars. *The Astrophysical Journal* 546:248–266.

Bernatowicz T., Fraundorf G., Tang M., Anders E., Wopenka B., Zinner E., and Fraundorf P. 1987. Evidence for interstellar SiC in the Murray carbonaceous meteorite. *Nature* 330:728.

Bradley J. 2003. The astromineralogy of interplanetary dust particles. *Lecture Notes in Physics* 609:217–235.

Bradley J. P. 2004. Interplanetary dust particles. In *Treatise on geochemistry,* vol. 1, edited by Davies A. M., Holland H. D., and Turekian K. K. Amsterdam: Elsevier. pp. 689–711.

Bradley J. P. and Brownlee D.E. 1986. Cometary particles: Thin sectioning and electron beam analysis. *Science* 231:1542–1544.

Brownlee D. E., Hörz F., Hrubsch L., McDonnell J. A. M., Tsou P., and Williams J. 1994. Eureka!! Aerogel capture of meteoroids in space (abstract). Lunar and Planetary Science 25:183–184.

Brownlee D. E., Tsou P., Atkins K. L., Yen C.-W., Villinga J. M., Price S., and Clark B. C. 1996. Stardust: Finessing expensive cometary sample returns. *Acta Astronautica* 39:1–4; 51–60.

Brownlee D. E., Tsou P., Anderson J. D., Hanner M. S., Newburn R. L., Sekanina Z., Clark B. C., Hörz F., Zolensky M. E., Kissel J., McDonnell J. A. M., Sandford S. A., and Tuzzolino A. J. 2003. Stardust: Comet and interstellar dust sample return mission. *Journal of Geophysical Research* 108:8111.

Brownlee D. E, Hörz F., Newburn R. L., Zolensky M., Duxbury T. C., Sandford S., Sekanina Z., Tsou P., Hanner M. S., Clark B. C., Green S. F., and Kissel J. 2004. Surface of young Jupiter family Comet 81 P/Wild-2: View from the Stardust spacecraft. *Science* 304:1764–1769.

Burchell M. J., Thomson R., and Yano H. 1999a. Capture of hypervelocity particles in aerogel: In ground laboratory and low earth orbit. *Planetary and Space Science* 47:189–204.

Burchell M. J., Cole M. J., McDonnell J. A. M., and Zarnecki J. C. 1999b. Hypervelocity impact studies using the 2 MV Van de Graaff accelerator and two-stage light gas gun of the University of Kent at Canterbury. *Measurement Science and Technology* 10: 41–50.

Burchell M. J., Creighton J. A., Cole M. J., Mann J., and Kearsley A. T. 2001. Capture of particles in hypervelocity impacts in aerogel. *Meteoritics & Planetary Science* 36:209–221.

Burchell M. J., Creighton J. A., and Kearsley A. T. 2004. Identification of organic particles via Raman techniques after capture in hypervelocity impacts on aerogel. *Journal of Raman Spectroscopy* 35:249–253.

Crovisier, J., Leech, K., Bockelee-Morvan D., Brooke T. Y., Hanner M. S., Altieri B., Keller H. U., and Lellouch E. 1997. The spectrum of comet Hale-Bopp (C/1995 01) observed with the Infrared Space Observatory at 2.9 AU from the Sun. *Science* 275: 1904–1907.

Flynn G. J., Horz F., Bajt S., and Sutton S. R. 1996. In situ chemical analysis of extraterrestrial material captured in aerogel (abstract). Proceedings, 27th Lunar and Planetary Science Conference. p. 369.

Fujiwara A., Mukai T., Kawaguchi J., and Useugi K.T. 1999. Sample return missions to small bodies. *Advances in Space Research* 25: 231–238.

Fujiwara A., Abe M., Kato M., Kushiro I., Mukai T., Okada T., Saito J., Sasaki S., Yano H. and Yeoman D. 2004. Sample return science by Hayabusa near-Earth asteroid mission (abstract #1521). 35th Lunar and Planetary Science Conference. CD-ROM.

Gaffey M. J. 1999. Bias correction of the relative fluxes of the meteorite types: Asteroid spectroscopy and orbital dynamics. *Meteoritics & Planetary Science* 35:A57–58.

Gillet P., Biellmann C., Reynard B., and McMillan P. 1993. Raman spectroscopic studies of carbonates Part I: High-pressure and high-temperature behaviour of calcite, magnesite, dolomite and aragonite. *Physics and Chemistry of Minerals* 20:1–18.

Gounelle M. and Zolensky M. E. 2001. A terrestrial origin for sulfate veins in CI1 chondrites (abstract #1609). 32nd Lunar and Planetary Science Conference. CD-ROM.

Graham G. A., Kearsley A. T., Wright I. P., Grady M. M., Drolshagen G., McBride N. M., Green S. F., Burchell M. J., Yano H., and Elliott R. 2001a. Analysis of Impact residues on spacecraft surfaces: Possibilities and problems. *Proceedings of the Third European Conference on Space Debris*. pp. 197–203.

Graham G. A., Franchi I. A., Kearsley A. T., and Burchell M. J. 2001b. The use of a Raman microprobe in analysis of extraterrestrial material impacted into aerogel. *Proceedings of the Royal Microscopial Society* 36:251–254.

Graham G. A., Kearsley A. T., Butterworth A. L., Bland P. A., Burchell M. J., McPhail D. S., Chater R. J., Grady M. M., and Wright I. P. 2004. Extraction and microanalysis of cosmic dust collected during sample return missions: Laboratory simulations. *Advances in Space Research* 34:2292–2298.

Greenberg J. M. and Hage J. I. 1990. From interstellar dust to comets: A unification of observational constraints. *The Astrophysical Journal* 361:260–274.

Heymann D. 1987. Raman spectra of carbon in the Canyon Diablo iron meteorite (abstract). Proceedings, 18th Lunar and Planetary Science Conference. pp. 419–420.

Hörz F., Zolensky M. E., Bernhard R. P., See T. H., and Warren J. L. 2000. Impact features and projectile residues in aerogel exposed on Mir. *Icarus* 147:559–579.

Jones A. P., Claeys P., and Heuschkel S. 2000. Impact melting of carbonates from the Chicxulub impact crater. In *Impacts and the early Earth*, edited by Gilmour I. and Koeberl C. Lecture Notes in Earth Sciences, vol. 91. pp. 343–361.

Kawaguchi J., Useugi K., and Fujiwara A. 2003. The MUSES-C mission for the sample and return–Its technology development status and readiness. *Acta Asronautica* 52:117–123.

Kistler S. S. 1931. Coherent expanded aerogels and jellies. *Nature* 127:741.

Kistler S. S. 1932. Coherent expanded aerogels. *Journal of Physical Chemistry* 36:52–64.

Kurat G., Koeberl C., Presper T., Brandstatter F., and Maurette M. 1994. Petrology and geochemistry of Antarctic micrometeorites. *Geochimica et Cosmochimica Acta* 58:3879–3904.

McCumber D. E. and Sturge M. D. 1963. Linewidth and temperature shift of the R lines in ruby. *Journal of Applied Physics* 34:1682–1684.

Michel-Levy M. C. and Lautie A. 1981. Microanalysis by Raman spectroscopy of carbon in chondrites. *Meteoritics* 16:301–302.

Nakashima S., Katahama H., Nakakura Y., and Mitsuishi A. 1986. Relative Raman intensities of the folded modes in SiC polytypes. *Physical Review B* 33:5721–5729.

Papike J. J., ed. 1998. *Planetary materials*. Washington, D.C.: Mineralogical Society of America.

Popp J., Tarcea N., Keifer W., Hilchenbach M., Thomas N., Stuffler T., Hofer S., Stöffler D., and Greshake A. 2002. The effect of surface texture on the mineralogical analysis of chondritic meteorites using Raman spectroscopy. *Planetary and Space Science* 50:865–870.

Rietmeijer F. J. M. 1998. Interplanetary dust particles. In *Planetary materials*, edited by Papike J. J. Washington, D.C.:Mineralogical Society of America. pp. 1–95.

Tsou P., Brownlee D. E., Laurance M. R., Hrubesh L., and Albee A. L. 1988. Intact capture of hypervelocity micrometeoroid analogs (abstract). 19th Lunar and Planetary Science Conference. pp. 1205–1206.

Tsou P., Brownlee D. E., Sandford S. A., Hörz F., and Zolensky M. E. 2003. Wild-2 and interstellar sample collection and Earth return. *Journal of Geophysical Research* 108:8113.

Tuzzolino A. J., Economou T. E., Clark B. C., Tsou P., Brownlee D. E., Green S. F., McDonnell J. A. M., and Colwell M. T. S. H. 2004. Dust measurements in the coma of comet 81p/Wild-2 by the Dust Flux Monitor Instrument. *Science* 304:1776–1780.

Wang A., Jolliff B. L., and Haskin L. A. 1999. Raman spectroscopic characterization of a Martian SNC meteorite Zagami. *Journal of Geophysical Research* 104:8509–8519.

Westphal A. J., Snead C., Borg J., Quirico E., Raynal P.-I., Zolensky M. E., Ferrini G., Colangeli L., and Palumbo P. 2002. Small hypervelocity particles captured in aerogel collectors: Location, extraction, handling and storage. *Meteoritics & Planetary Science* 37:855–865.

Westphal A. J., Snead C., Dominguez G., Bradley J. P., Zolensky M. E., Flynn G., and Brownlee D. 2003. An extraction and curation technique for particles captured in aerogel collectors (abstract #1826). 34th Lunar and Planetary Science Conference. CD-ROM.

Wopenka B. 1988. Raman observations on individual interplanetary dust particles. *Earth and Planetary Science Letters* 88:221–231.

Wopenka B. and Sandford S. A. 1984. Laser Raman microprobe study of mineral phases in meteorites. *Meteoritics* 19:340–341.

Wynn-Williams D. D. and Edwards H. G. M. 2000. Proximal analysis of regolith habitats and protective biomolecules in situ by laser Raman spectroscopy: Overview of terrestrial Antarctic habitats and Mars analogs. *Icarus* 144:486–503.

Zinner E. 1998. Stellar nucleosynthesis and the isotopic composition of presolar grains from primitive meteorites. *Annual Reviews of Earth and Planetary Science* 26:147–188.

Zolensky M. E., Pieters C., Clark B., and Papike J. J. 2000. Small is beautiful: The analysis of nanogram-sized astromaterials. *Meteoritics & Planetary Science* 35:9–29.